# A System-Level Spacecraft Thermal Model Reduction Method Applicable to Transient Analysis

Toshihiro Shibukawa[1] and Shinichi Nakasuka[2]
*ArkEdge Space Inc., Koto-ku, Tokyo, 135-0063, Japan*

**To ensure proper operation of a spacecraft, it is important to perform thermal design so that the temperature of each component inside remains within the acceptable range. For spacecraft, which cannot be verified in actual environments using real hardware prior to launch, thermal design and validation is generally carried out using a thermal model created by software such as Thermal Desktop. To shorten the time required for thermal design, this study proposes a system-level spacecraft thermal model reduction method. This method automatically selects nodes to be reduced, preserves the physical meaning of the original model, and is suitable for both steady and transient analysis. In this study, the proposed method was applied to a 763-node thermal model of a CubeSat called ONGLAISAT, developed at the University of Tokyo. By investigating the trend of node condensation in the reduced models, and comparing the analysis time and the temperature analysis results between the original and reduced models for transient analysis cases, the effectiveness of the method was demonstrated.**

## Nomenclature

| | | |
|---|---|---|
| $c$ | = | specific heat |
| $C$ | = | heat capacity |
| $K$ | = | thermal conductance |
| $Q$ | = | heat input |
| $R$ | = | radiative coupling |
| $t$ | = | time |
| $T$ | = | temperature |
| $\lambda$ | = | thermal conductivity |
| $\rho$ | = | density |
| $\sigma$ | = | Stefan-Boltzmann constant |
| $\cdot^E$ | = | evaluation |
| $\cdot^F$ | = | filter |
| $\cdot^R$ | = | reduced |
| $\cdot_r$ | = | reference value |

| | | |
|---|---|---|
| TMM | = | Thermal Mathematical Model |
| GMM | = | Geometrical Mathematical Model |
| LR | = | Linear Regression |
| GP | = | Gaussian Process |
| TPWL | = | Trajectory Piece Wise Linear |
| TMRT | = | Thermal Model Reduction Tool |
| ROM | = | Reduced-Order Model |
| ANN | = | Artificial Neural Network |
| MB | = | Model-Based |
| DD | = | Data-Driven |
| TASA | = | Taiwan Space Agency |
| RSI | = | Remote Sensing Imager |
| AOCS | = | Attitude and Orbit Control System |

## I. Introduction

IN orbit, a spacecraft is surrounded by cosmic microwave background radiation, while also subjected to external heat flux such as solar radiation, albedo and planet infrared radiation, which can cause significant changes in the thermal environment depending on the spacecraft's orbit and attitude. Moreover, in vacuum environment, there is no convective heat exchange, and it is necessary to deal with heat input from the outer space environment and internal heat generation using only conductive and radiative heat exchange methods. To ensure proper operation of a spacecraft under such harsh conditions, it is crucial to perform thermal design to ensure that the temperature of the components inside remains within their allowable temperature range. The thermal engineer must utilize thermal control components appropriately, while adjusting the implementation and allocation of resources with other subsystems, such as structure, power, and attitude. Thermal design must be implemented so that all components remain within their allowable temperature range under all conditions and operational scenarios that may occur in orbit, and must be

[1] Engineer, Advanced Project Department, 3A, DOME ARIAKE HEADQUARTER, 1-3-33 Ariake, Koto-ku, Tokyo
[2] Professor, Department of Aeronautics and Astronautics, 7-3-1 Hongo, Bunkyo-ku, Tokyo

verified that it functions properly in the actual spacecraft. This is not an easy task and can be time-consuming even with the knowledge and experience of experts.

Since it is impossible to test the spacecraft in the actual space environment, spacecraft thermal design is generally conducted through analysis. Thermal analysis is generally performed using a Thermal Mathematical Model (TMM) based on the lumped parameter method which divides the spacecraft into nodes, and calculates the thermal equilibrium equations represented by Eqs. (1) and (2). When constructing a detailed TMM, it is difficult to manually calculate the radiative couplings between nodes and external heat inputs in orbit. Therefore, thermal analysis software such as Thermal Desktop® or ESATAN-TMS® are generally used. In these software, a Geometrical Mathematic Model (GMM) is created using a CAD interface, and the radiatives couplings are calculated from the geometrical information. Also, by setting orbit conditions for the GMM, external heat inputs can be calculated. Using these calculation results, as well as thermal conductance between nodes and internal heat generation data, a graph-like detailed TMM can be constructed. By solving the thermal equilibrium equations for this TMM, steady or transient analysis can be performed.

$$\mathbf{0} = \boldsymbol{Q_i} - \sum_{j=1}^{n} \boldsymbol{K_{ij}}\left(\boldsymbol{T_i} - \boldsymbol{T_j}\right) - \sum_{j=1}^{n} \boldsymbol{R_{ij}}\boldsymbol{\sigma}\left(\boldsymbol{T_i^4} - \boldsymbol{T_j^4}\right) \tag{1}$$

$$\boldsymbol{C_i}\frac{\boldsymbol{dT_i}}{\boldsymbol{dt}} = \boldsymbol{Q_i(t)} - \sum_{j=1}^{n} \boldsymbol{K_{ij}}\left(\boldsymbol{T_i(t)} - \boldsymbol{T_j(t)}\right) - \sum_{j=1}^{n} \boldsymbol{R_{ij}}\boldsymbol{\sigma}\left(\boldsymbol{T_i^4(t)} - \boldsymbol{T_j^4(t)}\right) \tag{2}$$

One of the issues of thermal analysis using these thermal models is the the analysis time required per run. Thermal analysis is repeatedly conducted in critical phases of thermal design, such as hardware design, uncertainty analysis, and thermal balance test model correlation. Therefore, shortening the analysis time per run can lead to a significant reduction in the overall time required for thermal design. Table 1 shows the number of typical thermal model nodes and required analysis time for each spacecraft size.

**Table 2. Typical Thermal Models**

| Spacecraft Size | Nodes | Run Time (LEO) |
|---|---|---|
| Conventional | $10^3 – 10^5$ | 1 – 10 hrs |
| Smallsats | $10^2 – 10^3$ | 10min – 1 hr |

As an example of a thermal model of a conventional-sized satellite, Figure 1 shows the GMM of Amazonia-1, a 637 kg remote sensing satellite developed in Brazil.[1] The TMM corresponding to this GMM consists of approximately 11,000 nodes, and takes about 10 hours to run a typical transient analysis case. In TMMs for such conventional-sized satellites, even running a single analysis case can take a considerable amount of time, becoming a temporal bottleneck in the thermal design process. Therefore, reducing analysis time directly leads to shortening the design process period.

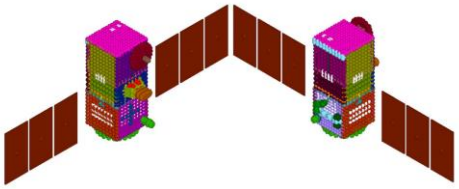

**Figure 1. GMM of Amazonia-1.**

On the other hand, the GMM of ONGLAISAT, a 6U CubeSat developed at the University of Tokyo, is shown in Figure 2.[2] The TMM consists of 763 nodes, and takes about 3 to 15 minutes to run a typical transient analysis case (5550 seconds), and the analysis time for TMM of smallsats is significantly shorter than that of conventional-sized satellites. However, the development period is also shorter for smallsats, and the total resources allocated as an entire satellite system is limited. It is desired to find a thermal design as optimal as possible in a short period, and a quick and detailed design parameter iteration is necessary to realize this. Therefore, even for smallsats, it is important to reduce the time required for each analysis run without sacrificing model accuracy, to perform repeated analysis to reach the optimal design solution.

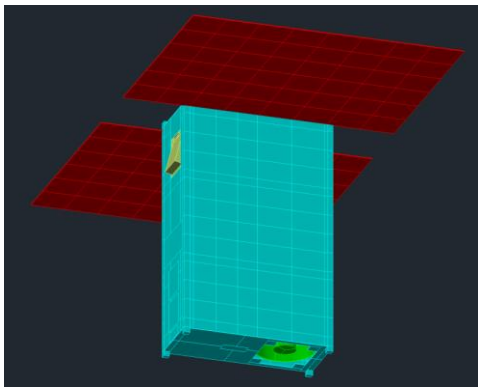

**Figure 2. GMM of ONGLAISAT.**

One way to shorten the analysis time is to reduce the number of nodes constructing the TMM. An extreme example of a fast-running TMM is a several-node model, which represents the entire spacecraft with only several nodes. In such a model, the analysis time is extremely short, taking only a few seconds or less, and is still sufficient to evaluate the amount of heat exchange between the entire spacecraft and the environment. Therefore, it is useful for designing the surface optical properties of spacecraft in the early stages of design. On the other hand, because the internal details of the spacecraft is not modeled, it cannot be used for more detailed design, such as implementation of heat pipes and gap fillers. It is also not possible to accurately evaluate the allowable temperature range, and evaluation must be

performed based on the component with the most severe conditions inside the spacecraft on a provisional basis. Therefore, a reduced model intended for use in the detailed thermal design process must have the characteristic of reducing the analysis time while maintaining analysis accuracy for each component inside the spacecraft, which is an intermediate between the detailed model and the several-node model.

## II. Model Reduction and Spacecraft Thermal Models

Not only for TMMs of spacecraft, but in general, analysis model reduction is commonly performed and can be divided into two main approaches: model-based and data-driven. In the model-based approach, a reduced model is constructed by integrating similar nodes or removing unnecessary nodes, maintaining the characteristics of the original model as much as possible under the same physical governing equations. This approach has the following advantages: 1. The reduced model can be used for hardware design and validation, 2. Steady and transient analyses can be performed using the same model, 3. It can be flexibly applied to multiple applications, and 4. The reduction results of the TMM can be feedbacked to creating reduced GMMs. On the other hand, in the data-driven approach, a reduced model is constructed by finding correlations or patterns between the inputs or design parameters of the original model and the outputs obtained by analysis. Typical methods include LR, DNNs, and GP. These methods have the following advantages: 1. The model size can be significantly reduced and very short analysis time can be expected, and 2. The reduced model can be constructed from input-output data alone.

A survey on model-based reduction methods in the fields of numerical mathematics, systems and control, and structural analysis was performed by Besselink et al.[3] Examples of methods covered by this survey are mode displacement methods, Krylov subspace based methods, and balanced truncation. Also, another method that is not introduced in this survey is Guyan static condensation.[4] As a method than can be applied to non-linear models, Trajectory Piecewise Linear approach (TPWL)[5] is representative.

As examples of applying these model-based reduction methods to spacecraft TMMs, Jouffroy, et al.[6], Molina and Clemente,[7] and Hugonnot et al.[8] all applied Guyan static condensation to TMMs. Especially in Ref. 8, detailed mathematical processes are described, and a tool called Thermal Model Reduction Tool (TMRT) was developed by Thales Alenia Space based on this method. Kim and Kim[9] also applied Guyan static condensation to a model created by COMSTAMP, a thermal analysis tool developed in Korea Aerospace Research Institute. In this study, LU decomposition was introduced to accelerate calculations, and a quantative index, which is the temperature difference between nodes, was also introduced to evaluate the thermal uniformity between two nodes. Also, comparison of analysis results between the original TMM and the reduced TMM was conducted to adjust parameters and correlate the reduced TMM. Deiml, et al.[10] developed three model reduction methods: Empirical Model Reduction Method, Matrix-Based Reduction Method, and Summation Method. However, details of these methods are not described.

Considering that TMMs are graph-like models, another approach to model reduction is graph clustering. By grouping nodes that have uniform characteristics, nodes in the same group can be condensed to one node. Especially, if the graph is not fully connected and can be divided into multiple connected components, clustering can be performed using connected component decomposition. One field where this approach applicable is electronic circuit analysis, where independent connected components can exist on the same circuit. Rommes and Schilders[11] decomposed a large electronic circuit network model into multiple components using connected component decomposition and performed node condensation or deletion for each component. Fernandez-Rico et al.[12] proposed a semi-autonomous spacecraft thermal model reduction process using connected component decomposition, focusing on the similarity between thermal mathematical models and electronic circuit analysis models. This study was the first to explicitly claim a quasi-autonomous process among model-based spacecraft TMM reduction methods. However, regarding the validation of the method, application was limited to steady analysis at the component level.

So far, previous studies on applying model-based methods for spacecraft TMM reduction have been introduced, but there are also many examples of applying data-driven methods. Hengeveld et al.[13] proposed a data-driven approach using GP to create a Reduced-Order Model (ROM) which captures the relationship between the input parameters of the original TMM and the output of the analysis. By using this method, it is possible to try thousands of combinations of parameters per second to perform uncertainty analysis, which is impossible to achieve with model-based methods. This method was turned into a software package called Veritrek and has already been applied to real missions such as the Mars 2020 Helicopter.[14] Reis-Junior et al.[1] proposed a method for constructing reduced TMMs using DNNs. While Hengeveld's method is only applicable to steady analysis, this study aimed to be applicable to transient analysis by using Recurrent Neural Networks, and it focuses particularly on the application to operational training and operational planning using SILS (Simulator-in-the-Loop) simulations. The results of applying the proposed method to Amazonia-

1's TMM were shown, but the reproducibility of transient cases was not high. Nishikawa et al.[15] proposed a method for constructing a low-cost reduced model using Lasso regression models. This research demonstrates that even with a simple Lasso regression model, high accuracy can be achieved for transient analysis by performing preprocessing and feature engineering. Unlike GP or DNN, it is not a complete black box model, so it is possible to quantitatively evaluate which inputs are most sensitive to specific temperature locations.

A summary of previous research on spacecraft TMM reduction is shown in Table 2, compared by the following factors.

- Model-based or data-driven
- Component-level applications or system-level applicatons
- (Quasi-)Autonomous or manual node selection and reduction
- Applicable to steady analysis or transient analysis

**Table 2. Previous Research on Spacecraft TMM Reduction.**

| ID | Author | Year | MB or DD | Component or System | Autonomous or Manual | Steady or Transient |
|---|---|---|---|---|---|---|
| 1 | Deiml, et al.[10] | 2015 | MB | Component | Unknown | Both |
| 2 | Fernandez-Rico, et al.[12] | 2016 | MB | Component | Autonomous | Steady |
| 3 | Hugonnot, et al.[8] | 2016 | MB | System | Manual | Both |
| 4 | Kim, et al.[9] | 2017 | MB | Component | Manual | Steady |
| 5 | Hengeveld, et al.[13] | 2017 | DD (GP) | System | Autonomous | Steady |
| 6 | Reis Junior, et al.[1] | 2021 | DD (DNN) | System | Autonomous | Transient |
| 7 | Nishikawa, et al.[15] | 2022 | DD (Lasso) | System | Autonomous | Transient |

Regarding the model-based methods, studies 1, 2, and 4 all deal only with reducing thermal models at the component-level, and have not been applied at the system-level of the spacecraft. The only study attempting to apply to a system-level model of a satellite, study 3, shows that it can also be used for transient analysis, but node selection is manually conducted by thermal designers. Therefore, a method that can be applied to transient analysis at the system-level of a satellite with autonomous node selection has not yet been established. On the other hand, all data-driven methods are applied to the system-level of the satellite, but there is a disadvantage that they cannot achieve one of the objectives of this study, which is to use the same reduced model in each process of thermal design.

In this study, a model-based spacecraft TMM reduction method which can maintain physical characteristics and parameters, and can be applied flexibly to thermal design processes was addressed. The method was aimed to be applied to the system-level TMM of the spacecraft, rather than just the component level. Moreover, to reduce the burden on operators and the dependence on experts, the selection of nodes to be reduced is autonomously performed. Finally, the reduced model created was aimed to be capable of both steady and transient analysis, and can be used for in-orbit analysis and operational simulation,. To achieve such characteristics, a method based on connected component decomposition, taking reference from study 2, was proposed. The benefits of connected component decomposition include its applicability to large-scale model reduction, relatively low computational cost, and the ability to automatically determine the number of nodes after reduction.

Novel elements of the proposed method in contrast to study 2 are as follows.

1) extension of the method to transient analysis and system-level by setting up analysis cases for temperature output of each node in node selection for reduction

2) extension of the method to system-level by considering radiation in determining and processing coupling with boundary nodes to maintain heat exchange between boundary nodes and other nodes

3) proposal of a hyperparameter selection method based on the required features of the reduced model

4) verification of the effectiveness of the method through consideration of the physical implications of the obtained reduced model, and its benefit in creating a reduced GMM.

## III. Thermal Model Reduction Process

### A. Overview of Method

To achieve the features previously mentioned, a model-based reduction method that integrates nodes with thermal homogeneity, which can be considered to have the same temperature, was examined. To determine groups of nodes with thermal homogeneity, an autonomous method based on the connected component decomposition, which was validated at the component-level and steady analysis in previous research[12], was extended for use in system-level and transient analysis. As mentioned previously, a spacecraft TMM is itself a graph-like model, so it is possible to apply

graph clustering methods directly to it. However, the TMM has two types of connections: thermal conductances and radiative couplings. In particular, radiative couplings contribute nonlinearly to the system, making it potentially difficult to use for proper reduction. Moreover, even if two nodes are connected by strong thermal conductances, if one node receives a large heat input, a large temperature difference may occur, and may be inappropriate to consider them thermally homogeneous.

Considering these issues, this study adopted an undirected graph that represents the thermal homogeneity between two nodes, and selected nodes to be condensed through connected component decomposition of this graph, and reduced the original TMM based on this result. To evaluate the thermal homogeneity between two nodes, the following two indices proposed in previous study[12] was utilized:

A. Whether the dimensionless thermal conductance is above a certain threshold, $p_f$

B. Whether the temperature difference for a particular analysis case is below a ceratin threshold, $\delta T_{max}$

Index A. involves sparsely processing the thermal conductance matrix, which is a parameter of the linear terms in the TMM, to make connected component decomposition easier. This is particularly useful as conduction is more dominant than radiation in internal heat exchange in spacecraft and is a useful indicator of thermal coupling. However, as mentioned earlier, even nodes connected by strong thermal conductance may have temperature differences between them due to heat input, making it difficult to consider them thermally homogeneous. Therefore, index B. is introduced to cover heat input imposed on the thermal model. This is a data-driven approach that partially incorporates the results of analyses using the original TMM into the model-based reduction method, and is expected to improve the effectiveness of the reduction. In the following sections, each of the processes in the model reduction method will be described in detail.

### B. Processing Thermal Conductance

The thermal conductance between nodes represents the connections within the thermal mathematical model network and serves as an effective indicator for evaluating thermal homogeneity. The thermal conductance is calculated based on the physical characteristics of each node, the distance between nodes, and the method of contact between nodes (in cases where each node is included in different materials or components). Therefore, the conductance value can vary widely, ranging from approximately $10^{-5}$ to $10^{3}$ W/K, depending on the differences in material and insulation design of the volumes or components represented by each node. In this reduction method, the strength of the thermal coupling between nodes represented by the conductance must be evaluated. Therefore, it is necessary to consider not only the absolute value of the conductance, but also the geometric and physical information of the nodes. For this purpose, a standard conductance matrix was calculated from the geometric configuration and thermal capacity of each node, and the thermal conductance was normalized by elements of this matrix.

First, to calculate the standard value for thermal conductance, distances between each node were calculated using the node coordinate matrix output from Thermal Desktop. Representative length was set using these node distances, and the standard conductance value was then calculated based on Fourier's law, assuming the material properties of A7075-T6, which is actually used in structural parts of spacecraft. Cross sectional area was converted to heat capacity using the reference material properties $\rho_r$ and $c_r$ using Eq, (3). By normalizing the thermal conductance using the calculated standard value, it can be interpreted as indicating how much heat transport due to conduction between the target nodes is significant relative to the structural parts of typical spacecraft.

$$C_i = \rho_r c_r V_i = 2\rho_r c_r S_i L_i \tag{3}$$

$$K_{ij}^{s} = \frac{\mu_r U_{ij}}{D_{ij}^2}, \qquad \mu_r = \frac{2\lambda_r}{\rho_r c_r}, \qquad \frac{1}{U_{ij}} = \frac{1}{C_i} + \frac{1}{C_j} \tag{4}$$

$$\widetilde{K}_{ij} = K_{ij}/K_{ij}^{s} \tag{5}$$

Once the normalized dimensionless thermal conductance matrix is calculated, each element is compared with $p_f$ to create the conductance filtering matrix. This matrix is a binary matrix, which shows the homogeonity between nodes based on thermal conductance.

$$\widetilde{K}_{ij}^{F} = \begin{cases} 1 \left(\widetilde{K}_{ij} > p_f\right) \\ 0 \left(\widetilde{K}_{ij} \le p_f\right) \end{cases} \tag{6}$$

### C. Processing Temperature Difference

In model-based TMM reduction methods, the reduced model also follows the thermal equilibrium equation. Within this equation, the heat input is the only input variable, which can be categorized into two types: (a) external heat input from the environment or from boundary nodes, and (b) heat generation at internal nodes of the thermal model.

In terms of the system-level TMM, (a) external heat input mainly comes from solar radiation, albedo, and the Earth's infrared radiation. These heat inputs vary greatly in amount and distribution depending on the spacecraft's attitude and surface optical properties. On the other hand, the internal heat generation of each component corresponds to (b) heat generation at internal nodes of the thermal model. Since there are as many combinations of heat generation as there are operation modes of the spacecraft, it is more complicated than at the component level, and the importance of transient analysis is higher than steady analysis. Therefore, in order to establish a model-based reduction method at the system level, it is important to be able to respond to various heat input conditions and to maintain sufficient analysis accuracy even in transient analysis. For this purpose, careful selection of analysis cases for calculating the temperature difference matrix is required. In this study, two types of analysis cases were set: "generic analysis cases" and "worst-case real scenario analysis cases," each corresponding to the two types of heat input.

The generic analysis cases are set up to address external heat input from the environment. The dominant external heat input is solar radiation, and the temperature of the entire spacecraft changes significantly depending on the direction of solar radiation. In addition, surface optical property design, which affects the magnitude of external heat input, is generally implemented on the structural panels with space exposure. Therefore, the external heat input conditions in the generic analysis cases are set to conditions where the sun is facing each structural panel. For example, for satellites with a rectangular shape with six panels such as CubeSats, a total of six generic analysis cases are set. Some of these analysis cases may not occur in the nominal operating state on orbit, but should be considered in situations where the satellite has lost attitude control, such as a tumbling state, where external heat input can come from all sides. The solar constant is set to the nominal value on the orbit of the subject satellite, which is 1366W/m$^2$ for an Earth orbiting satellite. In generic analysis cases, to minimize the effect of internal heat generation, the power state of all components are unified to the nominal state on orbit. For example, for an Earth orbiting satellite, the power state is set to the battery charging mode, and mission equipment and some communication modules that operate only for a certain period of time are turned off.

The worst-case real scenario cases simulate the worst hot or worst cold conditions among the operation scenarios actually assumed in orbit. In thermal design, the analysis results in the worst case are important for evaluating whether they exceed the allowable range, and therefore worst case accuracy is required in the reduced model. These worst conditions are difficult to evaluate in steady analysis, especially in the case of a satellite in orbit where the orbital conditions change every moment, and it is necessary to perform transient analysis using the actual assumed orbit conditions. On the other hand, the temperature difference matrix cannot be calculated for the entire transient result, so it is necessary to extract temperature information of each node at a specific moment. Therefore, a snapshot of the temperatures of every node are taken when a certain component reaches its highest or lowest temperature to evaluate the temperature difference. These analysis cases are especially intended to properly evaluate the worst hot conditions for components that exhibit high heat generation for only a specific period, such as communication modules and mission components, and the temperature accuracy in such conditions is preserved in the reduced model.

Given the temperatures of each node for case $n$ as $\boldsymbol{T^n}$, the temperature difference matrix can be calculated as below. Each element is compared with $\delta T_{max}$ to calculate the temperature filter matrix, which is also a binary matrix.

$$\Theta_{ij}^{n} = \left| T_i^n - T_j^n \right| \tag{7}$$

$$\Theta_{ij}^{F,n} = \begin{cases} 0 \left(\Theta_{ij}^{n} > \delta T_{max}\right) \\ 1 \left(\Theta_{ij}^{n} \leq \delta T_{max}\right) \end{cases} \tag{8}$$

**D. Handling Boundary Conditions**

One factor that has a significant impact on the output results of thermal models is the nodes set as boundary conditions (boundary nodes). If boundary nodes are not maintained separately from other nodes before and after model reduction, it can change the assumptions of the analysis. Therefore, a boundary condition filter that prevents boundary nodes from being integrated during the model reduction process is defined as Eq. (9). Here, $V^B$ represents the set of boundary nodes. With this boundary condition filter, boundary nodes are treated as non-homogeneous compared to all other nodes.

$$B_{ij}^{F,B} = \begin{cases} 1 \ (i,j \notin V^B) \\ 0 \ (i \in V^B \text{ or } j \in V^B) \end{cases} \tag{9}$$

To maintain accuracy after model reduction and preserve major physical parameters, it is also effective to maintain nodes with connections to boundary nodes (sub-boundary nodes) as much as possible. This is because it is important to maintain heat flux from boundary nodes to the model before and after reduction. Here, $V^S$ represents the set of sub-boundary nodes.

$$B_{ij}^{F,S} = \begin{cases} 1\ (i,j \notin V^S \text{ or } i,j \in V^S) \\ 0\ (i \in V^S, j \notin V^S \text{ or } i \notin V^S, j \in V^S) \end{cases} \tag{10}$$

In component-level thermal models, boundary nodes and sub-boundary nodes are mostly connected by thermal conductivity, and previous study[12] has used thermal conductivity coupling to determine sub-boundary nodes. On the other hand, in system-level thermal models, boundary conditions often involve heat exchange through radiation coupling, such as space or chamber walls, rather than thermal conductance. Therefore, determining sub-boundary nodes with thermal conductivity coupling is not possible. This study determined sub-boundary nodes based on heat flux through radiation coupling.

### E. Calculating Adjacency Matrix and Connected Components Decomposition

The adjacency matrix is calculated as the Hadamard product of the filters calculated so far.

$$A_{ij} = \widetilde{K}_{ij}^{F} \cdot B_{ij}^{F,B} \cdot B_{ij}^{F,S} \cdot \prod_{n} \Theta_{ij}^{F,n} \tag{11}$$

Connected components decomposition is conducted to this adjacency matrix by the Depth-First Search algorithm,. As a result, the number of nodes in the reduced model $n_r$, the reduction rate $r_r = n_r/n_d$, and the model transformation matrix $\boldsymbol{P}$ are calculated.

### F. Model Reduction and Evaluation

Parameters of the reduced model can be obtained by calculating the product of the parameters in the original model and the model transformation matrix.

$$\mathbf{K^R} = \mathbf{P^T K P} \tag{12}$$
$$\mathbf{R^R} = \mathbf{P^T R P} \tag{13}$$
$$\mathbf{C^R} = \mathbf{P^T C} \tag{14}$$
$$\mathbf{Q^{R,n}} = \mathbf{P^T Q^n} \tag{15}$$

By calculating the thermal equilibrium equation for the reduced model, the temperature outputs $\mathbf{T^{R,n}}$ can be obtained. A Crank-Nicolson solver was developed for this calculation. The accuracy of the model is evaluated by comparing the reduced model analysis results and the heat capacity weighted average of the original model analysis results $\mathbf{T^{E,n}}$. Eq. (16) shows the calculation of $T_i^{E,n}$, where $n_i$ is number of nodes in the original model that were condensed to node $i$ in the reduced model. The maximum temperature difference between the two temperatures for the evaluation node set $V^E$ in the evaluation case set $E^E$ is used as the evaluation factor $\delta T$ for reduced model error.

$$T_i^{E,n} = \frac{\sum_{j=1}^{n_i} T_j^n C_j}{\sum_{j=1}^{n_i} C_j}, i = 1, \dots, n_c \tag{16}$$

$$\delta T = \max_{n \in E^E, i \in V^E} \left| T_i^{E,n} - T_i^{R,n} \right| \tag{17}$$

### G. Hyperparameter Selection

To select the optimal reduced model for the user's requirements, hyperparameter search is done by grid search. Evaluation of each reduced model is done by the reduction rate $r_r$ and the model error $\delta T$. In this research, a threshold for the model error was set, and the reduced model that had the smallest number of nodes among the models that had a model error value lower than this threshold was selected as the optimal reduced model.

## IV. Application of Model Reduction to ONGLAISAT Thermal Model

### A. Overview of ONGLAISAT and its Thermal Model

ONGLAISAT (ONboard Globe-Looking And Imaging Satellite) is a 6U remote sensing satellite developed jointly by the University of Tokyo and the Taiwan Space Agency (TASA).[16] Figure 3 shows the arrangement of internal components and structural design. Because the satellite is scheduled to be released into orbit from the ISS, the seasonal β-angle variation is significant, and the eclipse rate ranges from 0% to about 39%. Under these conditions, the thermal control requirement of mission equipment at around 20℃ during operation is the largest thermal challenge, given the power constraints of CubeSats. In addition, as shown in Figure 3, the satellite structure is unique, with all internal components and all panels except the MX panel being fastened to the PX and MX frames. The components with high heat generation, which are the communication system and mission board, are fastened with gap fillers inserted between the MX panel to enhance thermal coupling.

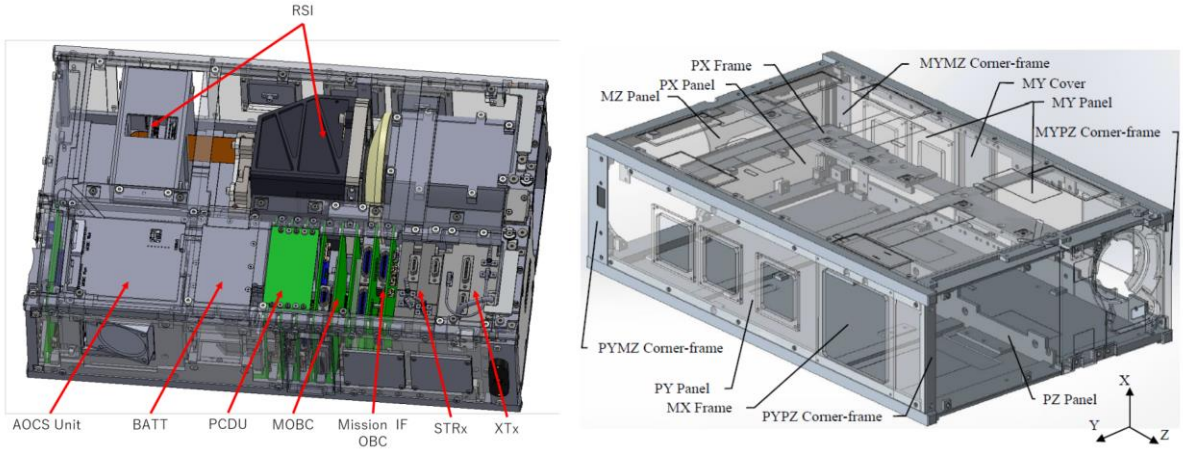


**Figure 3. Internal Component Arrangement (Left) and Structrual Design (Right) of ONGLAISAT.**

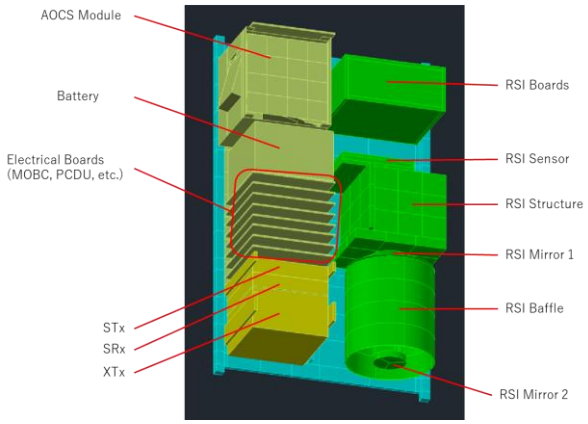


**Figure 4. Modeling of the Internal Components.**

**Table 3. Hyperparameter Grid Search Range**

| | |
|---|---|
| $p_f$ | {0.1, 0.2, 0.5, 1.0, 1.5, 2.0, 2.5, 3.0} |
| $\delta T_{max}$ | Every 0.1 in range 0.5 to 2.5 |

**Table 4. Nodes for Evaluation**

| Node Name | Remarks |
|---|---|
| XTx | High Heat Generation |
| STx | High Heat Generation |
| OBC | |
| Battery | Narrow Temperature Range |
| STT | Narrow Temperature Range |
| RSI Mainplate | Narrow Temperature Range |
| RSI Board | High Heat Generation |
| RSI Sensor | Narrow Temperature Range |
| RSI Mirror 1 | Narrow Temperature Range |
| RSI Mirror 2 | Narrow Temperature Range |

**Table 5. Environmental Settings**

| Parameter | Cold | Hot |
|---|---|---|
| Beta-angle [°] | 0 | 72 |
| Orbit Altitude [km] | 400 | 400 |
| Orbit Period [s] | 5554 | 5554 |
| Eclipse Duration [s] | 2160 | 0 |
| Solar Flux [W/m$^2$] | 1322 | 1412 |
| Albedo Rate [] | 0.25 | 0.35 |
| Earth IR Flux [W/m$^2$] | 211 | 267 |

To verify its effectiveness, the proposed method was applied to the detailed model used in the thermal design of ONGLAISAT. The exterior appearance of the GMM is already shown in Figure 2, and the modeling of the internal components is shown in Figure 4. Efforts were made in creating the GMM to model the unique satellite structure mentioned earlier in order to obtain accurate analysis results. The internal attitude control system module, communication system, battery, various boards, antennas, the mission module (RSI: Remote Sensing Imager)'s telescope and board, and the satellite structure and solar array panel (SAP) were modeled as precisely as possible. Each component or board inside is represented by one node, but the attitude and orbit control system (AOCS) module is modeled in detail to simulate the internal heat distribution, in particular the module's structure and each component inside. Also, the AOBC board included in the AOCS module has various types of elements, so unlike other boards, each of the heat-generating elements on the board were modeled in detail to analyze the temperature distribution on the board. The backplane board is also modeled in detail because of its large size and many connected boards that are likely to generate temperature distribution. Additionally, for the communication system, the brackets were modeled as accurately as possible to reproduce the thermal conductance. For the satellite structure, detailed models of the PX surface and MX surface were created, where the internal components are directly fastened, resulting in a large number of nodes. For the mission module, the number of nodes increased to express the temperature difference of the structural parts, based on the requirement to reduce the temperature difference.

## B. Settings for Reduction Process

Table 3 shows the hyperparameter grid search range for the ONGLAISAT thermal model. A total of 160 patterns of hyperparameter combinations were tested to output the reduction rate and temperature accuracy. Table 4 shows the set of nodes to evaluate the temperature accuracy. Representative nodes of the satellite bus and mission component were selected. The temperature accuracy threshold was set to 5.0℃. Table 5 shows the environmental settings for the cold and hot cases, and Table 6 shows the analysis cases used for handling temperature difference in the reduction process.

**Table 6. Case Setting for Reduction Process**

| Case Type | Case Name | Filter | Evaluation | Validation |
|---|---|---|---|---|
| Generic | PX Sun | ✓ | ✓ | |
| Generic | MX Sun | ✓ | ✓ | |
| Generic | PY Sun | ✓ | ✓ | |
| Generic | MY Sun | ✓ | ✓ | |
| Generic | PZ Sun | ✓ | ✓ | |
| Generic | MZ Sun | ✓ | ✓ | |
| Real Scenario | Battery Charge, Cold | | | ✓ |
| Real Scenario | Data Downlink, Hot | ✓ | | ✓ |
| Real Scenario | Mission, Cold | | | ✓ |
| Real Scenario | Mission, Hot | ✓ | | ✓ |
| Real Scenario | Safe Mode, Cold | ✓ | | ✓ |

## C. Reduced Model Output

The hyperparameters of the selected reduced model which met the temperature accuracy threshold of 5.0℃ and had the smallest reduction rate was $(p_f, \delta T_{max}) = (0.1, 1.8)$. The results of the grid search is shown in Figure 5. The total time required for the reduction process was 152.6 minutes.

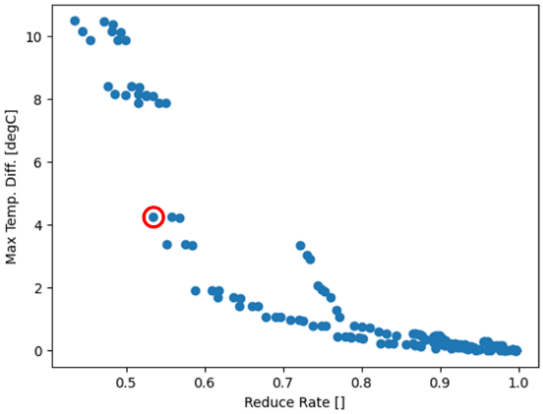


**Figure 5. Grid Search Results.**

Table 7 shows the the total number of nodes, thermal conductances, and radiative couplings of the selected reduced model. The number of nodes and thermal conductance were reduced to about 60%, and radiative couplings to about 45%. High reduction percentages were seen mainly in the satellite structures, especially in the PX panel/frame and the MX panel/frame. Insights into reduction results of these structures are described hereafter.

**Table 7. Node Reduction Results**

| Parameter | Original | Reduced |
|---|---|---|
| Nodes | 763 | 436 |
| Thermal Conductances | 1441 | 892 |
| Radiative Couplings | 18218 | 7877 |

Figure 6 shows the reduction results of the PX panel and frame. The PX panel is not directly fastened to the internal components, but is placed over the PX frame to prevent the interior of the satellite from being exposed to space. The surface property tapes are implemented on the PX panel as shown in Figure 7, and this distribution is also represented in the model. When comparing this distribution with the node reduction results in Figure 6, it can be seen that the trends match, and the temperature difference between these two areas due to the difference in surface properties is reflected in the node reduction results. Especially in the low-α and ε regions on the MZ side of the panel, where the amount of heat exchange with the environment is small, significant reduction is observed. On the other hand, the temperature distribution of the PX panel is found to be almost unaffected by the internal component heat dissipation. From this, insights that structural parts that are not directly fastened to the internal components of the satellite may be modeled relatively coarsely, can be attained.

The PX frame is thermally connected to many internal components. As a result, a detailed temperature distribution is present within the frame, and it can be seen that nodes are not as reduced as the PX panel. For the materials where

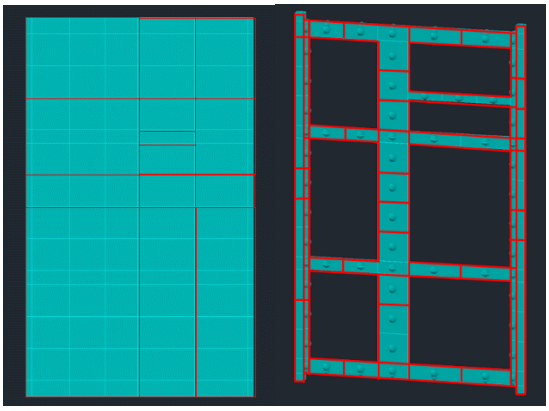

**Figure 6. Reduction Results of the PX Panel (Right) and PX Frame (Left).** *Nodes in the original model surrounded by the same rectangle are integrated to the same reduced node.*

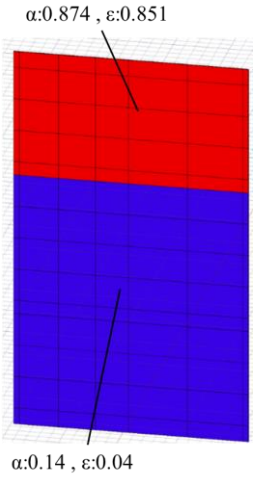


**Figure 7. Optical Properties of the PX Panel.**

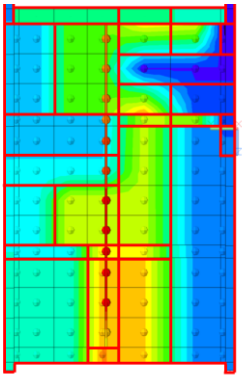

**Figure 8. Reduction Results of the MX Panel and Frame.** *Nodes in the original model surrounded by the same rectangle are integrated to the same reduced node.*

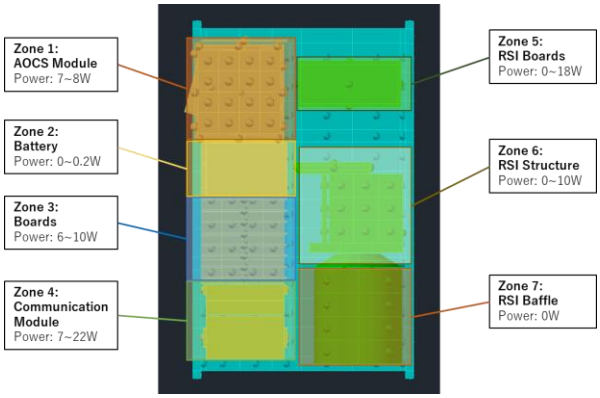


**Figure 9. Temperature Zones of ONGLAISAT.**

heat inflow is expected from various locations, data-driven recognition of temperature differences is used to automatically output the appropriate reduction rate to maintain the accuracy of the model after reduction.

Figure 8 shows the reduction results of the MX panel and frame, which are integrally molded, and the internal components are fastened to two rails at the Y-direction ends and a protrusion in the center of the panel. Looking at the node integration results in Figure 8, it can be seen that there is no temperature difference between the end rail and the panel portion due to this integral molding, and they are integrated as nodes. Additionally, the temperature zones of ONGLAISAT based on heating conditions and component types are shown in Figure 8, but comparing it with Figure 9, it can be seen that the node integration of the MX panel closely follows the thermal zones. Therefore, it is clear that the model reduction is being performed based on the qualitatively assumed thermal distribution.

The above discussion has focused particularly on the structural components of PX and MX, but by examining the node integration trends in areas where the reduction ratio is high, such as other structural components and mission components, one can gain an understanding of the characteristics of the original model and connect it to the manual reduction of thermal-geometric models. This is a unique advantage of this method, which can output reduced models that maintain physical properties while evaluating thermal homogeneity based on reference analysis results using data-driven methods. Furthermore, the integration results and discussions obtained thus far can be effectively utilized as insights when constructing thermal-geometric models corresponding to the reduced thermal mathematical model.

**Table 8. Analysis Time Comparison**

| Case Name | Case Period [s] | Original Model + SINDA/FLUINT® [s] | Original Model + C-N Solver [s] | Reduced Model + C-N Solver [s] |
|---|---|---|---|---|
| Battery Charge, Cold | 5,550 | 170.36 | 412.92 | 89.32 |
| Data Downlink, Hot | 5,550 | 175.39 | 418.10 | 90.68 |
| Mission, Cold | 11,100 | 960.00 | 879.90 | 185.42 |
| Mission, Hot | 11,100 | 1779.60 | 767.07 | 172.07 |
| Safe Mode, Cold | 11,100 | 355.75 | 1131.03 | 217.67 |

## D. Analysis Time Comparison

Table 8 shows the comparison of analysis time of the evaluation transient cases. These runtime results were obtained by an computer with an Intel® Core™ i9-10900K CPU @ 3.70 GHz and a RAM of 32.0 GB, and the analysis time considers only the runtime of the solver, and does not include any pre-processing or output steps.

Compared in the same Crank-Nicolson solver, the analysis time is shortened to approxmately 20%, and the effect of model reduction can be seen. Comparing the analysis time with SINDA/FLUINT®, which is the solver for Thermal Desktop®, analysis time is shortened to approxmately 50% for battery charge, data downlink, and safe mode cases. Since the mission cases have a heater control logic inside and the time step is shorter than other analyses, the analysis time with SINDA/FLUINT® is long as 30 minutes. For the reduced model with the Crank-Nicolson solver, the time step is fixed to one second, and therefore analysis time is about three minutes. This shows that model reduction is especially effective for analysis cases that require detailed heater control or include high heat input in a short period, since a shorter time step is set automatically in SINDA/FLUINT® for these cases.

## E. Temperature Output Comparison

Figures 10 to 12 shows the analysis results of transient analysis cases. The temperature accuracy is within 4.0℃ across all cases and is lower than the model error threshold. For the safe mode case (Figure 10), unstable temperature behavior is observed because the direction of the sun changes every moment due to tumbling. Even under this situation, the model error is within 2℃, and it can be said that the reduced model has robustness to solar direction due to the generic analysis cases.

Of the hot orbits cases (Figure 11), (a) shows the temperature of the XTx in the data downlink case. It can be seen that the XTx turns ON and consumes 15W for a period of 600 seconds, causing a rapid temperature increase. The temperature accuracy of XTx during this period is below 0.5℃, indicating that this reduced model can evaluate worst hot case conditions with high accuracy. On the other hand, when XTx is turned OFF and the attitude condition becomes steady in the PZ sun direction, it can be seen that the temperature accuracy of each component converges to a constant value.This shows that even in transient analysis, if the thermal input condition is constant, the model error converges and there is no possibility of divergence. This is one advantage of model-based methods, since divergence must be cared when using data-driven methods such as DNN.

Figures 11-(b) and 11-(c) show the mission operating case. It can be seen from Figure 11-(b) that the mission board generates heat of 11.4W for a short period of 250 seconds, and the temperature rises rapidly. The mission board shows

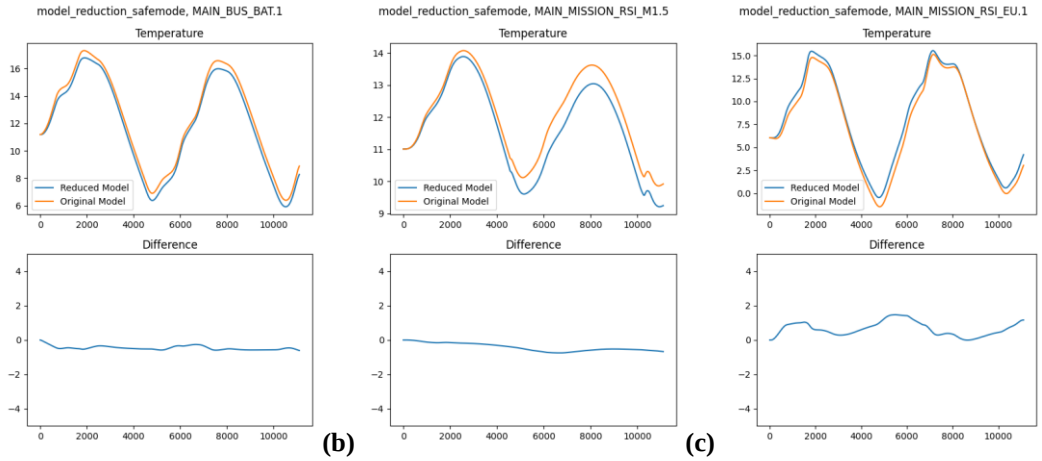


**Figure 10. Analysis Results in the Safe Mode Case.** *(a): Battery, (b): RSI Mirror 1, (c): RSI Board.*

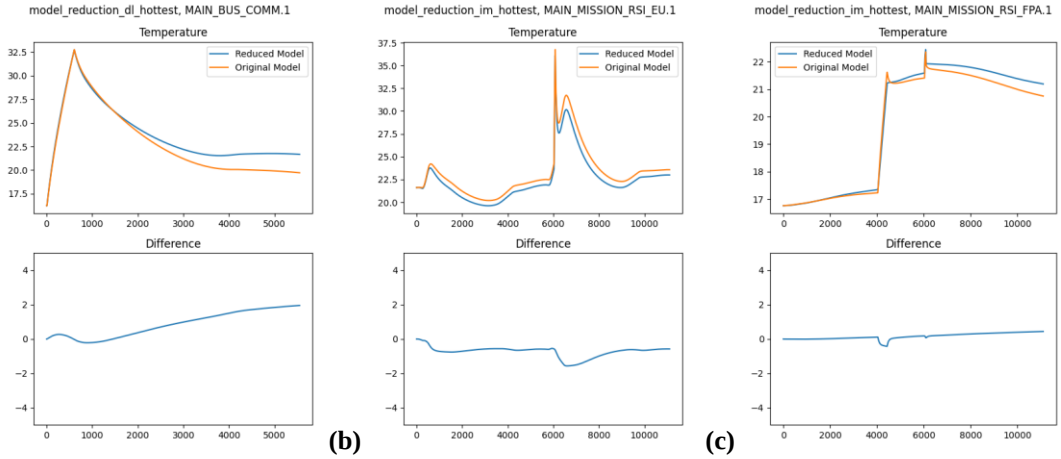


**Figure 11. Analysis Results in the Hot Orbit Cases.** *(a): XTx for Data Downlink, (b): RSI Board for Mission, (c): RSI Sensor for Mission.*

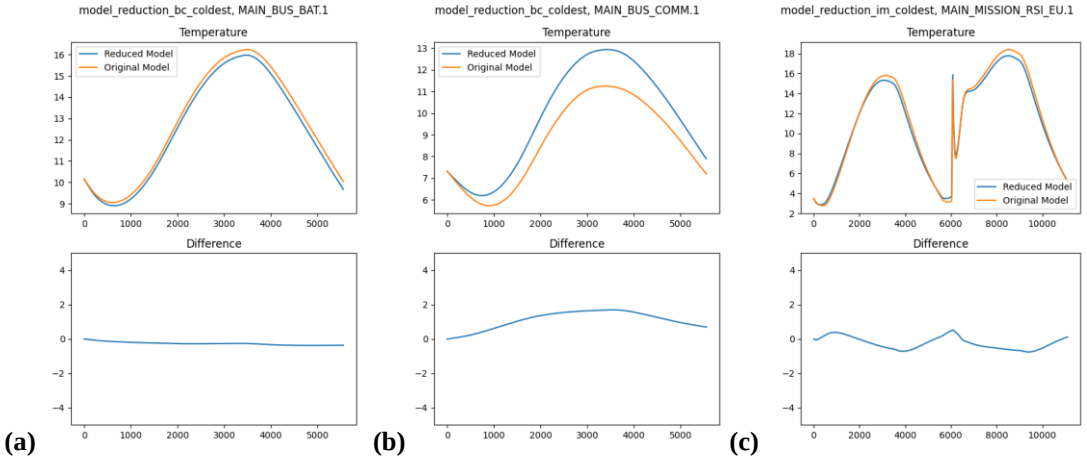


**Figure 12. Analysis Results in the Cold Orbit Cases.** *(a): Battery for Battery Charge, (b): XTx for Battery Charge, (c): RSI Board for Mission.*

a steeper temperature rise than the XTx board in Figure 11-(a) because it has a smaller heat capacity, but it is confirmed that the model error is small during this short period. For the mission sensor board in Figure 11-(c), the heater mounted on the bracket is controlled between 4,000 and 6,280 seconds, maintaining the temperature between 20℃ and 21℃. In the original model, the bracket was divided into six nodes, so a sharp temperature change was observed when the heater was turned on and off, but in the reduced model, the bracket was integrated into one node, and the heat capacity of the node where the heater is applied has increased, so the temperature change was not as sharp.

Figure 12 shows the analysis results for the cold orbit cases, which were not used in the process of model reduction. In both of these cases, the period from 3330 seconds to 5550 seconds is an eclipse period, and the external heat input becomes very small. Looking at each graph in Figure 12, the model error is below 2.0℃, and these results demonstrated that the reduced model obtained by this method can be used for various analysis cases without problems.

## F. Comparison with Manually Reduced Models

To demonstrate the efficiency of the proposed automatic reduction method compared to manual model reduction, five manually reduced models were prepared based on qualitative judgments for the thermal model of ONGLAISAT. Table 9 shows the components and structures targeted for manual reduction and which ones were targeted for each reduced model. Steady analyses for the generic cases were performed for these manually reduced models, same for those in the reduction process, and the reduction ratio and model error were plotted on the grid search results obtained by the proposed reduction method in Figure 13. The results showed that the automatically obtained reduced models were more efficient, demonstrating the effectiveness of node selection by data-driven methods.

**Table 9. Manually Reduced Models**

| Component | Nodes | | Reduced Model ID | | | | |
|---|---|---|---|---|---|---|---|
| | Original | Reduced | 1. | 2. | 3. | 4. | 5. |
| RSI Baffle | 16 | 1 | ✓ | ✓ | ✓ | ✓ | ✓ |
| RSI Structure | 33 | 5 | ✓ | ✓ | ✓ | ✓ | ✓ |
| PY Panel | 42 | 9 | ✓ | ✓ | ✓ | ✓ | ✓ |
| PX Panel | 98 | 24 | | ✓ | ✓ | ✓ | ✓ |
| MX Panel | 110 | 38 | | | ✓ | ✓ | ✓ |
| PX/MX Frame | 139 | 107 | | | | ✓ | ✓ |
| SAP | 96 | 24 | | | | | ✓ |
| Total Nodes | | | 687 | 613 | 541 | 509 | 437 |

## V. Conclusion

In this study, a model-based reduction method that is applicable to the system-level TMM of a spacecraft was developed, reducing the time required for thermal design and simplifying complex models. The method is automated by including a data-driven approach that determines the nodes to be reduced based on the analysis results obtained from the original model, and the reduced model can be applied to transient analysis. The method was established by focusing on the graph-like properties of TMMs and condensing thermally homogeneous nodes through graph clustering based on connected component decomposition. Furthermore, the information obtained from this reduction process can also be used for reducing the GMM, which can be considered as a secondary benefit.

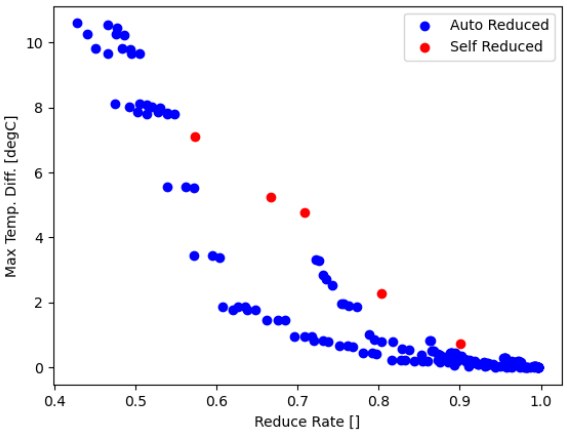


**Figure 13. Comparison of Manually Reduced Models.**

In applying connected component decomposition, an undirected graph that expresses thermal homogeneity between nodes was introduced using two evaluation indices: thermal conductance and temperature difference obtained from the analysis results. To demonstrate the effectiveness of the developed reduction method, it was applied to the 763-node system TMM of ONGLAISAT, developed at the University of Tokyo. The node reduction trend of the obtained reduced model was examined to validate that this method can preserve physical properties in the original model. Also by using this reduced model, it was demonstrated that analysis time can be shortened while maintaining analysis accuracy above a certain level, and can be applied in actual satellite development processes.

## References

[1]Reis Junior, J. D., Ambrosio, A. M., de Sousa, F. L., & Silva, D. F. (2021). Spacecraft real-time thermal simulation using artificial neural networks. Journal of the Brazilian Society of Mechanical Sciences and Engineering, 43, 1-17.

[2]Shibukawa, T., Nishimoto, S., Matsushita, S., Yokobori, S., Takashima, K., Ishikawa, A., Funase, R., & S. Nakasuka (2022). Thermal design approach for efficient development of cubesats with a common bus system. 51st International Conference on Environmental Systems.

[3]Besselink, B., Tabak, U., Lutowska, A., Van de Wouw, N., Nijmeijer, H., Rixen, D. J., ... & Schilders, W. H. A. (2013). A comparison of model reduction techniques from structural dynamics, numerical mathematics and systems and control. Journal of Sound and Vibration, 332(19), 4403-4422.

[4]Guyan, R. J. (1965). Reduction of stiffness and mass matrices. AIAA journal, 3(2), 380-380.

[5]White, J. K. (2003). A trajectory piecewise-linear approach to model order reduction of nonlinear dynamical systems (Doctoral dissertation, Massachusetts Institute of Technology).

[6]Jouffroy, F., Charvet, D., Jacquiau, M., & Capitaine, A. (2004). Automated thermal model reduction for telecom S/C walls. 18th Eur. Work. Therm. ECLS Softw., ESA/ESTEC, Noordwijk, The Netherlands.

[7]Molina, M., & Clemente, C. (2006). Thermal model automatic reduction: algorithm and validation techniques. SAE Transactions, 294-303.

[8]Hugonnot, P., Basset, T., Connil, P., Brunetti, F., & Ferrier, M. (2016, July). TMRT (Thermal Model Reduction Tool): Presentation of the tool and application on satellite model reduction for launcher coupled analysis. 46th International Conference on Environmental Systems.

[9]Kim, J. H. and Kim, B. (2017). Study on the reduction method of the satellite thermal mathematical model. Advances in Engineering Software, 108, 37–47.

[10]Deiml, M., Suderland, M., Reiss, P., & Czupalla, M. (2015). Development and evaluation of thermal model reduction algorithms for spacecraft. Acta Astronautica, 110, 168-179.

[11]Rommes, J. and Schilders, W. H. (2009). Efficient methods for large resistor networks. IEEE Transactions on Computer-Aided Design of Integrated Circuits and Systems, 29, 1, 28–39.

[12]Fernández-Rico, G., Pérez-Grande, I., Sanz-Andres, A., Torralbo, I., & Woch, J. (2016). Quasi-autonomous thermal model reduction for steady-state problems in space systems. Applied Thermal Engineering, 105, 456-466.

[13]Hengeveld, D., & Moulton, J. (2019, July). Uncertainty Quantification Using Reduced-Order Models. 49th International Conference on Environmental Systems.

[14]Moulton, J., Hengeveld, D., & Cappucci, S. (2020). Reduced-order modeling for rapid mission planning of the Mars 2020 Helicopter. Thermal & Fluids Analysis Workshop 2020.

[15]Nishikawa, T., Samir, K., Omata, N., Tsutsumi, S., Shibukawa, T., Nakasuka, S.(2022). Data-driven Thermal Reduced Order Model for Spacecraft On-board Prediction. Space Sciences and Technology Conference.

[16] Chan, C. Y., et al. (2022). Mission introduction of ONGLAISAT (ONboard Globe-Looking AI Satellite). 33rd International Symposium on Space Technology and Science.